Evaluating Long-term Seasonal Variability of Aerosol Optical Properties in Colorado

Erin K. Boedicker[1,2], Andre Bergeron[3], Gerardo Carrillo-Cardenas[4], Dominik Kulakowski[3], John Rogan[3], Elisabeth Andrews[1,2], A. Gannet Hallar[4]

[1]NOAA Earth System Research Laboratory, Boulder, CO 80305, USA
[2]Cooperative Institute for Research in Environmental Sciences, University of Colorado, Boulder, CO 80309, USA
[3]Graduate School of Geography, Clark University, Worcester, MA 01016, USA
[4]Department of Atmospheric Sciences, University of Utah, Salt Lake City, UT 84112, USA

Correspondence to: Gannet Hallar (Gannet.Hallar@utah.edu)

Abstract. Aerosol particles resulting from both wildfires and dust events introduce considerable uncertainty into both climate research and public health assessments. These challenges are becoming particularly evident in the western U.S. To gain a deeper understanding of western U.S. aerosol properties, we analyzed 13 years (2011-2024) of surface in-situ aerosol optical data from Storm Peak Laboratory (SPL) in northwestern Colorado, and 6 years (2019-2024) of surface in-situ aerosol optical data from Table Mountain (BOS) in central Colorado. The aerosol optical properties at both sites demonstrate a strong summer wildfire smoke signal (peaking in August) and evidence of springtime dust events. BOS exhibited higher aerosol loading than SPL, particularly during spring and winter, consistent with the proximity of BOS to urban sources and its lower elevation. While the general patterns observed for SPL are consistent with a previous climatological analysis (covering the period 2011-2016) for the site, the longer SPL dataset used here shows that there has been a significant increase in extreme wildfire smoke events for 2017-2024 relative to 2011-2016. Both summer and fall exhibit statistically significant increasing trends in the upper percentiles of scattering coefficient with trends of $10 \pm 1\%$ yr[-1] at the 98th percentile in the summer and 2.4 ± 0.4 % yr[-1] at the 96th percentile in the fall. Co-variability among some of the aerosol optical properties is used to further identify aerosol types and temporal patterns, demonstrating similarities between the two sites.

1 Introduction

The western U.S. climate has undergone significant changes over the past several decades (Westerling et al., 2006) marked by warming (Higuera and Abatzoglou, 2021), drought (Leeper et al., 2022), and declining snowpack (Mote et al., 2018). These environmental changes have led to enhanced wildfire activity (Pederson et al., 2013; Westerling et al., 2006), intensity (Iglesias et al., 2022; Mote et al., 2018), and increases in annual burn area (Dennison et al., 2014; Weber and Yadav, 2020), resulting in declining air quality conditions (Hallar et al., 2015; McClure and Jaffe, 2018; Wilmot et al., 2021). These shifts are closely linked to earlier springtime warming (Mote et al., 2018; Pederson et al., 2013) which strongly influences spring and summertime land surface aridity and aerosol loading (Hallar et al., 2017; Lian et al., 2020; Wilmot et al., 2021). Changes in

surface aridity can lead to an increased exposure to in airborne dust (Achakulwisut et al., 2019; Lambert et al., 2020; Pu and Ginoux, 2017) and particulate matter from wildfires, which can result in increased rates of respiratory illnesses (Delfino et al., 2009; Haikerwal et al., 2016), hospital admissions (Liu et al., 2015, 2017), and mortality rates (Johnston et al., 2012).

In addition to human health concerns, wildfire and dust-induced atmospheric aerosol particles impose notable effects on the climate system (Kok et al., 2023; Penner et al., 1992). For instance, aerosol particles can absorb and scatter solar radiation which inflict direct influences on the planetary energy balance (Bond et al., 2013; Ghan and Schwartz, 2007). They also have an indirect influence due to their ability to act as both ice and cloud condensation nuclei (Barry et al., 2021; Hallar et al., 2017; Jahn et al., 2020; Twohy et al., 2021; Wei et al., 2019). The chemical composition, size distribution, shape, and other external variables (e.g., relative humidity and wavelength of incident light) determine the aerosol optical properties (Seinfeld and Pandis, 2006) and can be used to characterize plumes that travel with air masses in the atmosphere (Davulienė et al., 2024; Junghenn Noyes et al., 2022).

Determining the radiative properties of aerosol particles caused by dust and wildfires requires an understanding of the aerosol properties as well as atmospheric transport mechanisms (Davulienė et al., 2024), and meteorological conditions (Wilmot et al., 2021). However, due to the high spatiotemporal variability of aerosol particles and sensitivity to climate, land use change, land management policies, and human activity (Ford et al., 2018), the radiative impact of aerosol particles remains uncertain (IPCC, 2023; Jiang et al., 2020; Kok et al., 2023).

In the western U.S., concentrations of natural and anthropogenic aerosol particles can vary significantly (Eibedingil et al., 2021; Hand et al., 2024). In regions with complex topography such as Colorado regional and synoptic-scale meteorology and climate conditions strongly influence aerosol transport from diverse sources (Creamean et al., 2016). On the more local scale, thermally driven upslope flow can lift pollutants from lower elevations to higher in the atmosphere (Collaud Coen et al., 2018).

Surface aerosol in-situ measurements provide aerosol information that is critical for quantifying aerosol climatology (temporal patterns, amount and characteristics) at a specific location (Laj et al., 2020). These measurements can be used to estimate direct and indirect aerosol radiative forcing and to infer additional information such as aerosol type (Cappa et al., 2016; Schmeisser et al., 2017). Long term aerosol measurements can also allow diagnosis of trends and identification of the changes contributing to those trends.

Japngie-Green et al. (2019) examined seasonal cycles of aerosol optical properties between 2011 and 2016 at Storm Peak Laboratory (SPL), an atmospheric science research laboratory near the Steamboat Springs ski resort in northwestern Colorado (Borys and Wetzel, 1997; Hallar et al., 2025). SPL is characterized as a mountain-top field site far from traffic, industry, or other anthropogenic influences and is often within the free troposphere (Collaud Coen et al., 2018; Japngie-Green et al., 2019). The work of Japngie-Green et al. (2019) established a baseline for aerosol optical property data measurements at SPL, revealing higher aerosol scattering and absorption coefficient patterns in the summertime due to increased wildfire activity and decreased springtime aerosol scattering Ångström exponent patterns related to dust events. Japngie-Green et al. (2019) analyzed the first six years of aerosol optical properties from SPL, however the long-term annual trends in aerosol

65 optical properties were not specifically evaluated, as six years of data is not long enough for a trend analysis (Collaud Coen et al., 2020). In this study, a longer data set (2011-2024) from SPL was utilized and data from the Table Mountain Field Site (BOS), another Colorado site with identical aerosol instrumentation as SPL, was also incorporated. BOS is located 120 km southeast of SPL on Colorado's Front Range (an urban corridor just east of the Rocky Mountains) and is within the boundary layer where most anthropogenic emissions take place. Data from these two sites was used to evaluate the climatological

70 patterns of aerosol optical properties measured in the region. Specifically, this study aimed to identify the similarities and differences in aerosol properties at SPL and BOS and to discuss how location impacts the long-term patterns observed at each site. Additionally, this study used aerosol optical properties to characterize wildfire activity and dust events in the region.

2 Methods

2.1 Sites

75 Surface aerosol in-situ data from two sites in Colorado was used: Storm Peak Laboratory and the Table Mountain Field Site. Both sites are part of the NOAA Federated Aerosol Network (NFAN), a collaborative network of sites that make long-term measurements of surface in-situ aerosol optical properties worldwide (Andrews et al., 2019). The NFAN sites have similar inlet and aerosol system infrastructure, operational and data processing protocols, and calibrations that follow established GAW aerosol sampling protocols to ensure consistent high-quality measurements that are directly comparable across sites in

80 the network (Andrews et al., 2019; WMO, 2016). The location of the sites, their proximity to population centers in Colorado, and topographical information is shown in Fig. 1. For the analysis presented herein, the primary data time ranges used are 2011-2024 for SPL and 2019-2024 for BOS; when different time ranges are used it is noted.

2.1.1 Storm Peak Laboratory

The first in-situ dataset used in this study was from Storm Peak Laboratory (40.455 N, 106.745 W, 3220 m asl). SPL is a high

85 elevation research facility (Hallar et al., 2025) located on the west summit of Mount Werner in the Park Range of the Rocky Mountains (Fig. 1). The site is 1120 m above and ~5 miles (~8 km) from the nearest population center of Steamboat Springs, CO (population ~13,500). Measurements at SPL started in 1981 and the facility is currently operated by the University of Utah. Measurements of in-situ aerosol optical properties began in 2011.

2.1.2 Table Mountain Field Site

90 The second aerosol in-situ dataset was from the Table Mountain Field Site (40.125 N, -105.237 W, 1689 m asl). BOS is ~10 km north of the nearest population center of Boulder, Colorado (population ~105,900; Fig. 1) and 50 km northwest of Denver, Colorado (population ~715,000). BOS has been a radio frequency test site since 1954; measurements of in-situ aerosol optical properties began in September of 2019. The site is managed by the National Telecommunications and Information Administration (NTIA), and the NFAN site is operated by NOAA's Global Monitoring Laboratory (GML).

95
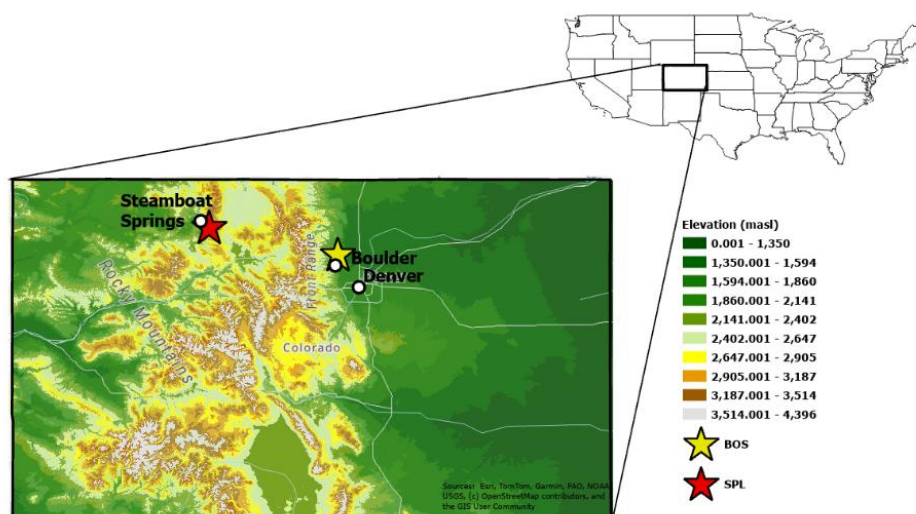
Figure 1. 30-meter Digital Elevation Model of Colorado with relative locations of SPL and BOS. Topographic data used is from the Shuttle Radar Topography Mission described by Farr et al. (2007).

2.2 Sampling conditioning and instrumentation

100 Aerosol particles at both SPL and BOS are sampled from 10 m above the surface to minimize contamination from local activities. At BOS, when needed, the sample air is gently heated (<40 C) to achieve a sample RH ≤ 40%. Malm et al. (2024) suggests this level of heating would not lead to volatilization of the BOS aerosol. At SPL, bringing the cool outside air into the heated observatory is enough to ensure the sample RH ≤ 40%. A switched impactor system provides size-segregated measurements using Berner-type multijet cascade impactors for 10 μm (~7 μm aerodynamic diameter) and 1 μm (~0.7 μm

105 aerodynamic diameter) size cuts (Berner et al., 1979). Switching between PM_{10} and PM_1 occurs every 6 minutes, yielding a 30-minute measurement of each size-cut per hour. Optical measurements at both sites are made at 1-minute resolution; here hourly averaged data is used. Prior to averaging, all measurements underwent a quality assurance process to remove contaminated values (e.g. spikes from ski area operations at SPL and mowing operations at BOS that are not representative of the wider region) and invalid values (e.g. when instruments failed).

110 Aerosol scattering (σ_{sp}) and backscattering (σ_{bsp}) coefficients are measured at both sites using an integrating nephelometer (Model 3563, TSI Inc.). The nephelometer measures aerosol scattering and backscattering coefficients at three wavelengths: 450, 550, and 700 nm. Total scattering coefficient is measured over an angular range of 7 – 170 degrees and total backscattering coefficient is measured over an angular range of 90 – 170 degrees. The nephelometer measurements were corrected for angular truncation and other instrument non-idealities using the method described by Anderson and Ogren (1998).

115 The nephelometer data is adjusted to standard temperature and pressure (0°C, 1 atm).

At SPL, aerosol absorption coefficients (σ_{ap}) were measured using both a Particle Soot Absorption Photometer (PSAP; Radiance Research), from 2011 - 2018, and a Continuous Light Absorption Photometer (CLAP; NOAA; Ogren et al., 2017), from 2011 - 2024. Both instruments measure absorption at three wavelengths: the PSAP at 467, 530, and 660 nm, and the CLAP at 467, 528, and 652 nm. The two instruments have previously been shown to be comparable measurements (Ogren et al., 2017), and an intercomparison of the PSAP and CLAP data from SPL was done to confirm this (**Section S1**). For the analysis presented in this work, only the CLAP data from SPL were used. The work done by Japngie-Green et al. (2019) used data from both the PSAP (2011 – 2013) and the CLAP (2013 – 2016), but the assessment in **Section S1** indicates that the CLAP absorption data presented here is comparable to the combination of PSAP and CLAP data presented by Japngie-Green et al. (2019). Only a CLAP was deployed at BOS and those are the data used. Absorption measurements were corrected for scattering and filter artifacts, sample area, flowrate, and non-idealities in the manufacturer's calibration (Bond et al., 1999; Ogren, 2010). The absorption data are reported at standard temperature and pressure, so no STP correction is needed. In the analysis presented, the wavelengths of all absorption coefficients (σ_{ap}) were adjusted to match the nephelometer scattering wavelengths (450, 500, and 700 nm) using the measured spectral dependence of absorption (**Section S2**).

2.3 Calculated parameters

Using the measured scattering and absorption coefficients, several variables can be calculated: single scattering albedo (SSA), backscattering fraction (BFR), scattering Ångström exponent (SAE), and absorption Ångström exponent (AAE). The equations for these variables are given below:

$$SSA = \frac{\sigma_{sp}}{(\sigma_{sp} + \sigma_{ap})} , \tag{1}$$

$$BFR = \frac{\sigma_{bsp}}{\sigma_{sp}} , \tag{2}$$

$$SAE = -\log\left(\frac{\sigma_{sp,\lambda1}}{\sigma_{sp,\lambda2}}\right) / \log\left(\frac{\lambda_1}{\lambda_2}\right) , \tag{3}$$

$$AAE = -\log\left(\frac{\sigma_{ap,\lambda1}}{\sigma_{ap,\lambda2}}\right) / \log\left(\frac{\lambda_1}{\lambda_2}\right) , \tag{4}$$

In Eq. 3 and Eq. 4, λ represents wavelength, and the subscripts indicate the specific wavelengths used in the calculation - both SAE and AAE were calculated using the 450 and 700 nm wavelength. These calculated parameters were only considered when constraints were met: $\sigma_{sp} > 1$ Mm^{-1} and/or $\sigma_{ap} > 0.5$ Mm^{-1}. These constraints were applied to the parameters that used the σ_{sp} and/or σ_{ap} values in their calculation (e.g. for SAE only the σ_{sp} constraint was applied but for SSA both constraints were applied). Below those values the calculated parameters are more heavily influenced by instrument noise and are less reliable. This filtering predominately affected parameters related to absorption (SSA and AAE). The SPL data was more heavily impacted as the site has lower overall aerosol loadings, resulting in filtering out over 50% of the potential SSA and AAE values being. Despite this filtering, the overall statistical values for the variables were not significantly affected (**Table S2**). This was

145   also shown by Schmeisser et al. (2017) who applied the same constraints to SPL data for the time period 2012-2013 (their supplemental table S5).

The measured σ_{sp} and σ_{ap} parameters depend on aerosol loading while the calculated parameters (SSA, BFR, SAE, and AAE) are independent of aerosol loading and instead describe characteristics of the aerosol. For atmospheric aerosol particles SSA typically ranges from 0.3 to 1 and provides information on aerosol composition and reflectivity (Laj et al., 2020).

150   SSA values near 1 are representative of low/non-absorbing "white" aerosol particles, while low SSA values <0.85 indicate darker, more-absorbing aerosol particles (Bond et al., 2013). BFR is sensitive to the smallest accumulation mode particles (diameter<0.3 µm; Collaud Coen et al., 2007). If the accumulation mode shifts to larger sizes, BFR will decrease and vice versa. Typically, BFR ranges from 0.08-0.2. SAE also yields information about the size distribution of aerosol particles (Schuster et al., 2006). Low values (SAE<1) indicate the presence of coarse particles, while high values (≥2) correspond to an

155   aerosol dominated by fine-mode aerosol particles. The absorption Ångström exponent can yield information about particle composition (Russell et al., 2010) with values near 1 associated with black carbon and higher values (≥2) representative of dust or smoke.

2.4 Trend analysis

Following a similar approach to McClure and Jaffe (2018), quantile regression was used to assess trends in extreme events at

160   SPL (R package quantreg). This method was developed by Koenker and Bassett (1978), and the software package used herein follows Koenker and D'Orey (1987). Quantile regression applies asymmetric weighting at different quantiles and regresses the entire dataset at specific quantiles to estimate the rate of change across the entire distribution of data (Koenker, 2005; Koenker and Hallock, 2001). This method is appropriate in situations where the data have significant outliers that would not be well characterized using symmetric weighting, such as that done in ordinary least squares regressions. This analysis was

165   performed on the σ_{sp} and SAE data, to assess changes in both aerosol amount and type. The same filtering used for the calculated optical properties was applied to σ_{sp} and SAE before this analysis to minimize effect of noise on the trends in the lowest quantiles. Trends using this method were considered significant when the p-value was < 0.05. The seasonal trend of Mm-1/yr was converted to % y-1 using the appropriate percentile of the seasonal values from the first year with σsp data as the baseline: 2011 for the winter, spring, and summer and 2012 for the fall. Trend analysis was not performed on the BOS

170   data as the time series was too short.

3 Results and Discussion

3.1 Climatology of aerosol optical properties at SPL and BOS

Mean annual PM$_{10}$ σ$_{sp}$ and σ$_{ap}$ at both field sites follow similar seasonal patterns with differences in overall magnitude (**Fig. 2 & 3**). While measurements were made at both PM$_{10}$ and PM$_1$ size cuts, the discussion here centers on the PM$_{10}$ measurement.

175   Average sub-micron fractions for σ$_{sp}$ were 0.8 ± 0.2 and 0.7 ± 0.1 for SPL and BOS and for σ$_{ap}$ the sub-micron fractions were

0.8 ± 0.2 and 0.8 ± 0.1 for SPL and BOS respectively (**Fig. S2**) indicating that 70-80% of the σ_{sp} and σ_{ap} are due to the PM_1 aerosol. Both σ_{sp} and σ_{ap} exhibited pronounced seasonal patterns with periodic low values occurring every winter (Dec – Feb) and peaks occurring in the summer into the early fall (June – Sep). Observed seasonal patterns for SPL's σ_{sp} and σ_{ap} generally agree with those previously reported by Japngie-Green et al. (2019). While similar seasonal patterns were observed at both

180 sites, BOS exhibited higher σ_{sp} and σ_{ap} values at all wavelengths and across all months for both PM_{10} and PM_1 data (**Fig. S3**). Specifically, at BOS the σ_{sp} and σ_{ap} values were up to a factor of 2 to 3 higher than those measured at SPL, depending on month and size cut. The largest differences between SPL and BOS in both σ_{sp} and σ_{ap} were observed in the winter (**Fig. S4**). These differences in magnitude are likely due to both the regional urban influences at BOS, and the elevation gradient between the two sites. Evidence for this can be seen in the diurnal variability at the two sites (**Fig. S5**). SPL's lower σ_{sp} and σ_{ap} values

185 and weaker diurnal cycles (particularly in winter) are largely due to the site's high elevation causing air masses measured at SPL to frequently be decoupled from the polluted boundary layer (Andrews et al., 2011; Collaud Coen et al., 2018). The slight increase in diurnal variability at SPL in the summer is likely due to thermally driven upslope flow, which is also consistent with the overall increase in σ_{sp} and σ_{ap} during those months. BOS exhibits a diurnal cycle throughout the year as it resides within the boundary layer where most anthropogenic emissions take place. This also results in the higher overall PM_{10} σ_{sp} and

190 σ_{ap} values at BOS.

While the seasonal cycle of σ_{sp} and σ_{ap} (high in summer, low in winter) occurred over the entire period of measurement at both sites, there was noticeable interannual variability with respect to the magnitude of the cycles (**Fig. 2**). This variability was largest in the summer months, likely associated with episodic wildfires. At both sites the influence of extreme wildfire events is not difficult to distinguish from baseline air pollution as aerosol loading is significantly higher during smoke events

195 (ranging from a factor of 2 higher to an order of magnitude higher depending on intensity of the smoke). Increases in aerosol loading associated with intense smoke events align well between the two sites (**Fig. 2**). Most long-range smoke observed at these two sites is transported eastward from western North America and impacts both sites. However, a notable exception occurred in May 2023 during transport of Canadian wildfire smoke into the U.S. For this event, the aerosol increase was larger at BOS as a result of the smoke being channelled down the Front Range of the Rocky Mountains with limited upward and

200 westward transport to SPL (see 2023 BOS σ_{sp} and σ_{ap} spike in **Fig. 2**).

The influence of outlier events on the temporal cycles in aerosol loading is apparent in the monthly mean values of σ_{sp} and σ_{ap}, as shown in **Fig. 3**. In the summer months at both sites, monthly mean values of σ_{sp} and σ_{ap} fall at the edge or above the interquartile range indicating a skew in the data towards higher loading for those months. To investigate the influence of extreme events on the data, simple outlier testing was done for the σ_{sp} upper bound, and a value of 50 Mm^{-1} was determined

205 to be appropriate to use for both sites (**Table S3**). Overall, July – September had the most hours with σ_{sp} exceeding 50 Mm^{-1} and these months dominated most years in terms of number of hours over the 50 Mm^{-1} threshold (**Fig. S6**, **Table S4**). There were notable exceptions at SPL, where June 2011 & May 2023 had the highest number of hours over 50 Mm^{-1} which could be the result of dust and/or wildfire events. In the SPL data, it is clear that the number of hours with extreme values per year is increasing. This is not discernible in the shorter BOS time series.
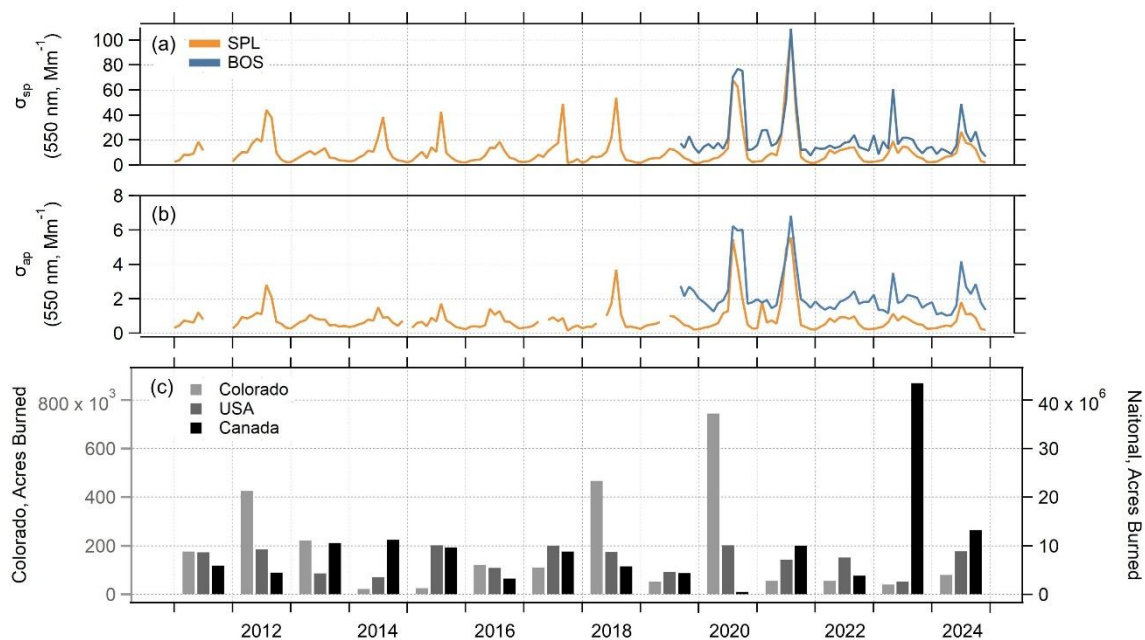
Figure 2. Top plots show average monthly cycles of PM_{10} σ_{sp} and σ_{ap} for 550 nm, from 2011 to 2024 for SPL (orange) and 2019 to 2024 for BOS (blue). The bottom plot shows data on yearly acres burned for Colorado (left axis), the United States, and Canada (national values on the right axis) from their respective fire incident databases: Rocky Mountain Area Coordination Center (RMACC), National Interagency Coordination Center (NICC), and the Canadian Wildland Fire Information System (CWFIS).
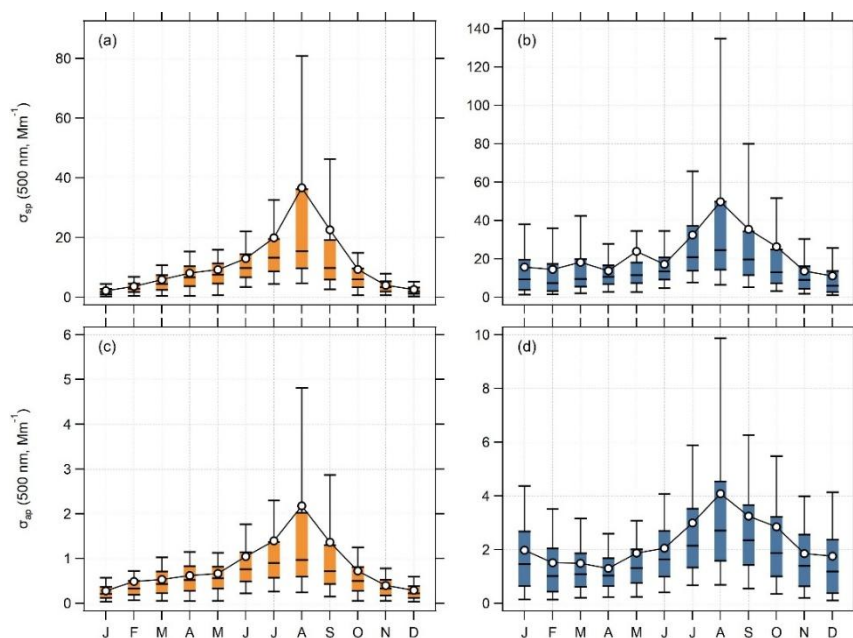
Figure 3. Seasonal cycles of PM_{10} σ_{sp} (550 nm) for **(a)** SPL and **(b)** BOS, and seasonal cycles of PM_{10} σ_{ap} (550 nm) for **(c)** SPL and **(d)** BOS. The solid lines with markers indicate the mean values, while the box-whiskers represent the percentiles (10th, 25th, median, 75th, and 90th). Note the differences in y-axis ranges.

220 **Table 1:** Seasonal values for σ_{sp}, σ_{ap}, SAE, AAE, SSA, and BFR. The average (μ), standard deviation (σ), and median (η) are reported. The seasons are defined by the following monthly bounds: winter is Dec- Feb, spring is Mar – Apr, summer is Jun – Aug, and fall is Sep – Nov. For SPL, statistics are reported for both the entire data range (2011 – 2024) and the shorter data range (2011-206) investigated by Japngie-Green et al. (2019) for comparison.

		SPL (2011-2024) $\mu \pm \sigma$ (η)	SPL (2011-2016) $\mu \pm \sigma$ (η)	BOS (2019-2024) $\mu \pm \sigma$ (η)
σ_{sp} (Mm⁻¹)	Winter	3 ± 3 (2.13)	3 ± 3 (2.41)	10 ± 20 (7.38)
	Spring	10 ± 10 (6.17)	8 ± 8 (6.84)	20 ± 40 (10.68)
	Summer	20 ± 100 (12.22)	20 ± 160 (12.18)	30 ± 50 (18.96)
	Fall	10 ± 30 (5.84)	10 ± 10 (5.73)	20 ± 63 (13.22)
σ_{ap} (Mm⁻¹)	Winter	0.3 ± 0.9 (0.25)	0.4 ± 0.3 (0.31)	2 ± 2 (1.22)
	Spring	0.6 ± 0.6 (0.50)	0.6 ± 0.6 (0.55)	2 ± 2 (1.15)
	Summer	2 ± 3 (0.87)	1 ± 2 (0.82)	3 ± 3 (2.15)
	Fall	1 ± 1 (0.50)	0.7 ± 0.9 (0.49)	3 ± 4 (1.88)
SAE (450 & 700 nm)	Winter	1.6 ± 0.6 (1.63)	1.7 ± 0.5 (1.71)	1.6 ± 0.5 (1.69)
	Spring	1.4 ± 0.5 (1.42)	1.4 ± 0.5 (1.42)	1.5 ± 0.5 (1.50)
	Summer	1.9 ± 0.4 (1.90)	1.8 ± 0.4 (1.91)	1.7 ± 0.3 (1.76)
	Fall	1.8 ± 0.4 (1.81)	1.8 ± 0.4 (1.87)	1.6 ± 0.5 (1.69)
AAE (450 & 700 nm)	Winter	1.4 ± 0.4 (1.38)	1.3 ± 0.4 (1.35)	1.4 ± 0.2 (1.37)
	Spring	1.5 ± 0.4 (1.52)	1.5 ± 0.2 (1.45)	1.4 ± 0.3 (1.39)
	Summer	1.3 ± 0.4 (1.34)	1.2 ± 0.3 (1.25)	1.2 ± 0.3 (1.21)
	Fall	1.6 ± 0.4 (1.53)	1.4 ± 0.3 (1.39)	1.4 ± 0.3 (1.41)
SSA (550 nm)	Winter	0.9 ± 0.1 (0.88)	0.88 ± 0.05 (0.89)	0.9 ± 0.3 (0.87)
	Spring	0.92 ± 0.03 (0.92)	0.92 ± 0.03 (0.92)	0.90 ± 0.05 (0.91)
	Summer	0.93 ± 0.02 (0.93)	0.93 ± 0.02 (0.93)	0.90 ± 0.04 (0.91)
	Fall	0.92 ± 0.03 (0.92)	0.91 ± 0.03 (0.92)	0.9 ± 0.1 (0.89)
BFR (550 nm)	Winter	0.2 ± 0.2 (0.16)	0.2 ± 0.2 (0.16)	0.16 ± 0.04 (0.16)
	Spring	0.2 ± 0.1 (0.15)	0.2 ± 0.2 (0.14)	0.15 ± 0.03 (0.15)
	Summer	0.15 ± 0.05 (0.16)	0.16 ± 0.02 (0.16)	0.15 ± 0.03 (0.15)
	Fall	0.16 ± 0.07 (0.16)	0.17 ± 0.07 (0.16)	0.15 ± 0.05 (0.15)

225

3.2 Trends in aerosol σ_{sp} and SAE at SPL

Long-term seasonal analysis of PM_{10} σ_{sp} at SPL suggests that overall aerosol loading is decreasing, with the majority of quantiles showing decreasing trends in all seasons except the fall (Fig. 4a). This is generally consistent with other trend analyses for aerosol scattering coefficient (Collaud Coen et al., 2020) and aerosol extinction coefficient (Hand et al., 2020) in the U.S. Differences were observed in the trends between seasons and over different data quantiles (**Fig. 4 & S7**). In all seasons, PM_{10} σ_{sp} values in and below the 70th quantile had significant but small observable changes (less than $\pm$ 2% yr^{-1}, **Table S5**). At the higher percentiles, trends were more pronounced indicating that changes in PM_{10} σ_{sp} are being driven by extreme events (**Fig. 4a**). For the seasonal analysis of SAE, significant trends were generally decreasing and larger in the lower quantiles for all seasons except the summer (**Fig. 4b**). A decreasing trend in SAE indicates an increased contribution from coarse mode aerosol.

Trends in the winter and spring showed decreases in extreme PM_{10} σ_{sp} events, with average significant trends of -2.4 $\pm$ 0.2 and -1.7 $\pm$ 0.4% yr^{-1} in and above the 80th quantile. This could be the result of a decrease in the intensity of dust events, or a decrease in background aerosol overall given that the winter and spring exhibited similar trends in and below the 70th quantile (average significant trends of -1.7 ± 0.3 and -1.6 $\pm$ 0.3% yr^{-1}). In these seasons, SAE trends above the 80th quantile were minimal and not significant (**Fig. 4b, Table S6**). In contrast, the SAE in the winter and spring had average significant decreasing trends in SAE of -1 ± 1 and -0.5 ± 0.2% yr^{-1} in and below the 70th quantile that were significant indicating an increase in coarse mode aerosol.

The summer and fall upper quantile data exhibited the largest trends in σ_{sp}, corresponding to significant increases in aerosol loading during extreme events (i.e. wildfire smoke). This was also observed by McClure and Jaffe (2018), who reported an increase in the 98th quantile particulate matter ($PM_{2.5}$) concentrations of 1.77 $\pm$ 0.68% yr^{-1} for the Northwest region of the United States. They attribute the increase to wildfire activity based on similar trends in total carbon and AOD observed in their study. Here, an increase in PM_{10} σ_{sp} of 10 $\pm$ 1% yr along with an increase in SAE of 1.4 $\pm$ 0.2% yr^{-1} at the 98th percentile was observed in the summertime at SPL indicating increased loadings of smaller particles consistent attributable to wildfire activity. The fall had a significant trend in the σ_{sp} 96th quantile of 2.4 $\pm$ 0.4% yr, but no significant trends in the upper quantiles of SAE to indicate changes in aerosol size (**Table S5**). The increasing fall trend for σ_{sp} may be due to wildfire season extending further into the autumn months (Goss et al., 2020).

The summer and fall trend attributable to smoke is also apparent in the fire data for Colorado. Previous source analysis of SPL data (Hallar et al., 2015; Japngie-Green et al., 2019) focus on data collected prior to 2016. At that time, the 2012 wildfire season was regarded as one of the most severe seasons impacting Colorado, marked by extreme dry winter conditions, hot summer temperatures and intense wildfire activity (Val Martin et al., 2013). Prior to 2017, the 2012 season also had two of the ten largest wildfires in Colorado history. Since then, there have been significant increases in the size and number of fires in Colorado according to data reported by the Rocky Mountain Area Coordination Center (RMACC, **Fig. 2c and Fig. S8**). As of 2024, the 2020 fire season is now regarded as the most severe with the three largest fires in Colorado history occurring

during that year. Additionally, much of the smoke impacting Colorado comes from outside of the state and the wider western

260   U.S. has also experienced exponential growth in wildfire frequency and area burned (Burke et al., 2021; Weber and Yadav, 2020).
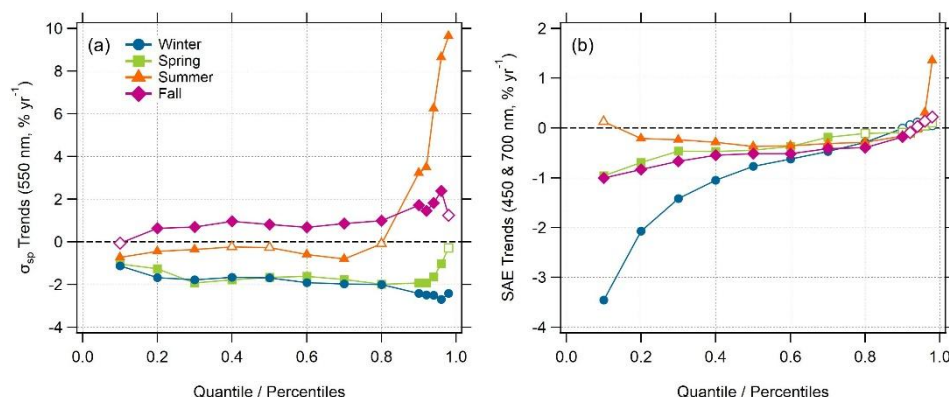
Figure 4: Quantile regression trends for PM$_{10}$ **(a)** σ$_{sp}$ and **(b)** SAE at SPL over all seasons. Winter = Dec – Feb, Spring = March - May,
265   Summer = June - Aug, Fall = Sept - Nov. Open markers show trends that were not significant at α = 0.05. Numerical values and *p*-values for the quantile regression trends are provided in **Table S5** & **S6**.

3.3 Aerosol classification using optical properties

3.3.1 Seasonality of derived optical properties

270   Qualitative information on the general seasonality of aerosol composition and size can be inferred from calculated aerosol optical properties. For readability, the figures below present just the PM$_{10}$ data, but the seasonal cycles for all variables are similar for the PM$_1$ size cut (**Fig. S9**). The seasonal patterns for the 2011-2024 SPL calculated aerosol optical properties are consistent with those previously reported for SPL for the 2011-2016 period (Japngie-Green et al., 2019; their Fig. 5) as discussed in more detail below.

275   PM$_{10}$ scattering Ångström exponent and backscatter fraction both decrease in the spring at SPL and BOS, indicating a shift towards larger particles (Schuster et al., 2006; **Fig. 5a, 5d**). The decrease in the sub-micron scattering fraction during the spring also shows increased influence from coarse mode particles (**Fig. S2c**). These changes are likely due to dust transport to the sites in the spring (Augustine et al., 2008; Hallar et al., 2015; Japngie-Green et al., 2019). The relationship between SAE and BFR during summer months is more complicated. SAE increases in all summer months, however, BFR increases in June

280   – and July at SPL – before decreasing for the rest of the summer. Increases in both SAE and BFR during the early summer indicate an increased contribution from smaller particles. As BFR and SAE are sensitive to different parts of the aerosol size distribution, the higher sub-micron contribution (increased SAE) with increased large accumulation mode particles (decreased BFR) later in the summer could indicate a narrowing of the size distribution (Collaud Coen et al., 2007). Alternatively, the

relationship could also indicate changes in the number or relative importance of different aerosol size modes if the particle size

285   distribution is multi-modal (Schuster et al., 2006).

Aerosol single scattering albedo tends to be lower in the fall and winter months and higher in the spring and summer months. The high SSA values in July and August are consistent with aged smoke aerosol where gases associated with the smoke have had the opportunity to condense resulting in a larger, more reflective aerosol (Andrews et al., 2004; Bian et al., 2020; Yokelson et al., 2009). Both sites exhibit a local SSA minimum in June – though the minimum is more pronounced at

290   BOS – indicating aerosol particles are slightly more absorbing during the early summer.

The aerosol absorption Ångström exponent is composition dependent, with different aerosol types having distinct ranges. Theoretically, black carbon (BC) aerosol has an AAE value of 1 while dust aerosol generally has an AAE value ≈ 2 (Bergstrom et al., 2007). Wildfire smoke plumes are typically expected to have AAE values ≥ 2 depending on fuel types and transport time (Forrister et al., 2015; Selimovic et al., 2018). At both sites, the PM_{10} AAE is highest in the spring and fall, with

295   a seasonal low in the summer (**Fig. 5b, S10**). The average spring and fall AAE values range from 1.4 - 1.6 (**Table 1**), which aligns with literature value ranges for dust and large particle / BC mixed aerosol (Lee et al., 2012; Schmeisser et al., 2017). The average AAE summer values range from 1.2 - 1.3 (**Table 1**), which is consistent with a mixture of anthropogenic biomass burning and BC dominated aerosol particles (Schmeisser et al., 2017; their table 1 & 4).

The impact of intense smoke plumes in the summer is not clear in the AAE monthly climatology depicted in **Fig. 5b**

300   (i.e., AAE is not > 2). This is likely due to the mixing of isolated biomass burning plumes with background air and other emissions. Clarke et al. (2007) were able to sample pollution and biomass burning plumes during flights over North America and reported the distribution of AAE for these plumes along with regional background (their Fig. 6). The distributions for all summer SPL and BOS hourly AAE data (**Fig. S11**) were most similar to the distribution reported for regional background by Clarke et al. (2007) but were broader indicating that multiple indistinguishable sources could be present. Summer distributions

305   showed more frequent high values of AAE than in the spring. Looking at AAE in relation to month and as a function of σ_{sp}, AAE was high (> 2) during high aerosol loading in the summertime which is consistent with the presence of smoke plumes (**Fig S12c, S12d, S13**). It can also be seen that in the springtime there were both dust (AAE ≥ 2, for high σ_{sp}) and pollution (AAE ≤ 1, for high σ_{sp}) plumes, with pollution having a higher impact at BOS than dust during that season (**Fig. S13**).

While the seasonality of AAE at SPL is similar to that reported in Japngie-Green et al. (2019), median AAE values

310   were higher from April to November relative to the period they considered (**Fig. 5b**). The AAE shift in the summer and fall is clearly attributable to the increase in extreme events with high AAE values (**Fig. 4 & S13**), however, the AAE increase in springtime could be the result of either an increase in dust events, overall decrease in background aerosol, or some combination of the two. For example, in their analysis of data from 2000 – 2016, Hand et al. (2019) observed significant decreases in $PM_{2.5}$ leading to an increase in the relative contribution of coarse aerosol mass over the continental U.S. but also found that mean

315   coarse mass in some regions did increase significantly over time. Without quantitative chemical data it is difficult to discern which process is driving changes in the optical properties at SPO and BOS. Additionally, while Japngie-Green et al. (2019) show SPL PM_1 AAE values being consistently lower than those of PM_{10}, this study observed PM_1 AAE values that were equal

to or higher than those calculated for PM_{10} from August to November (**Fig. S9 & S10**). This is likely in response to the overall decrease in aerosol particles at SPL (**Section 3.2**), and a shift in the sub-micron composition towards larger, less absorbing

320 particles. Support for this can also be seen in the overall decrease in sub-micron σ_{sp} and σ_{ap} fractions compared to the 2011-2016 period, indicating an increase in the impact of larger particles (**Fig. S2c & S2f**). This kind of shift in size has been previously observed at other sites within the continental U.S. (Sherman et al., 2015). Additionally, PM_1 SSA at SPL increased from August to November (**Fig. S10**) relative to the 2011-2016 time period, indicating that aerosol particles have become less absorbing overall. SSA was lowest during the late fall and winter (Oct – Feb), which is attributable to increased anthropogenic

325 emissions during colder months. Both AAE and SSA values were generally lower at BOS than at SPL, as a result of the geographical proximity of urban sources to BOS described in Section 3.1.
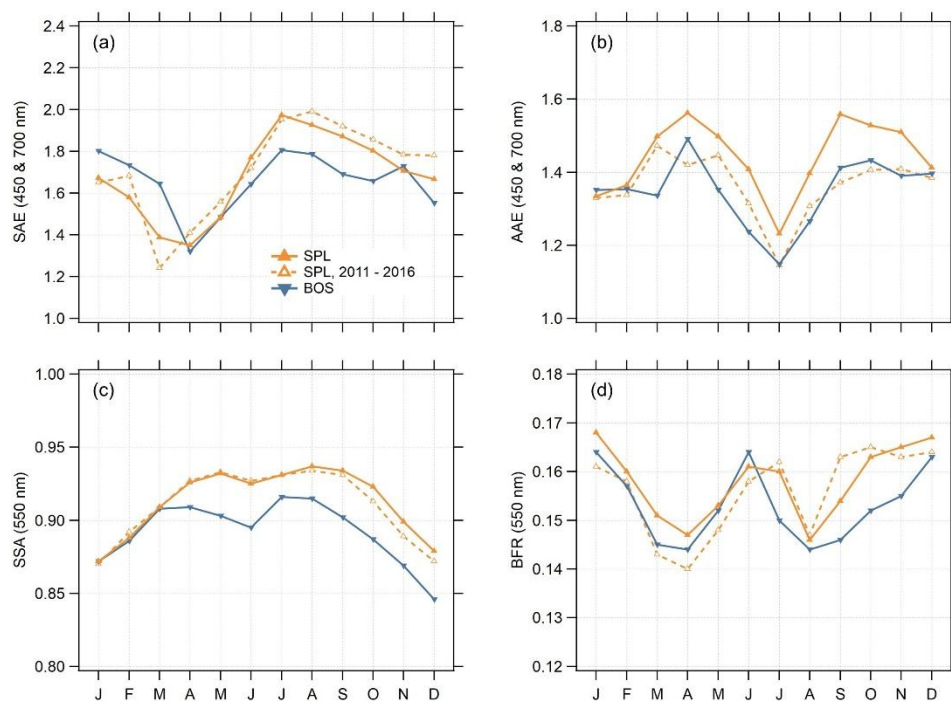
Figure 5. Monthly median PM_{10} (a) SAE for 450 & 700 nm, (b) AAE for 450 & 700 nm, (c) SSA for 550 nm, and (d) BFR for 550 nm. The
330 orange traces represent SPL data, with the solid line representing data from the entire measurement period (2011-2024) and the dashed line with open markers representing data from the shorter period (2011-2016) analyzed by Japngie-Green et al. (2019). The blue trace shows data from BOS (2019-2024).

3.3.2 Systematic variability of derived optical properties

335 Systematic variations between SAE and σ_{sp}, and AAE and SAE have previously been used to classify in situ aerosol types and sources (Cappa et al., 2016; Hallar et al., 2015; Schmeisser et al., 2017). Here analysis of the relationship between AAE and BFR is also explored.

The relationship between SAE and σ_{sp} at SPL showed two, seasonally distinct aerosol populations (**Fig. 6a**). In the spring (green-hued lines, Fig. 6), SAE decreased with increased σ_{sp} indicating an increase in particle size with higher aerosol

340 loadings which is consistent with dust. In the summer and early fall (orange and magenta hued lines, Fig. 6), SAE increased with increased σ_{sp} indicating a decrease in particle size at higher loadings which is consistent with biomass burning (Hallar et al., 2015). The spring SAE and σ_{sp} relationship at BOS **(Fig. 6b)** was less defined than that observed at SPL. At BOS, a similar decrease in SAE for lower aerosol loadings is observed, however, as loading increases the relationship changes and SAE begins increasing sharply. BOS is therefore likely sampling dust plumes that are either less intense and/or mixed with other aerosol

345 types (e.g., background, biomass burning, or anthropogenic outflow). During the summer and fall at BOS, the SAE and σ_{sp} relationship is consistent with biomass burning aerosol as the dominant aerosol type at the site.

The negative relationship between AAE and BFR also suggests influence from biomass burning **(Fig. 6c, d)**. The higher AAE and lower BFR are more likely to occur during smoke events due to the impact of condensed organics on the wavelength of absorption and the increase in accumulation mode diameter due to the condensation of those organics and other

350 co-emitted vapors. In contrast, smaller particles (higher BFR values) associated with AAE values near 1 are likely representative of the background air at these sites. This pattern (decreasing AAE with increasing BFR) is visible at both sites in the summer and early fall. In contrast, during the spring and winter values of AAE tend to be more consistent across all BFR values (**Fig S12**).
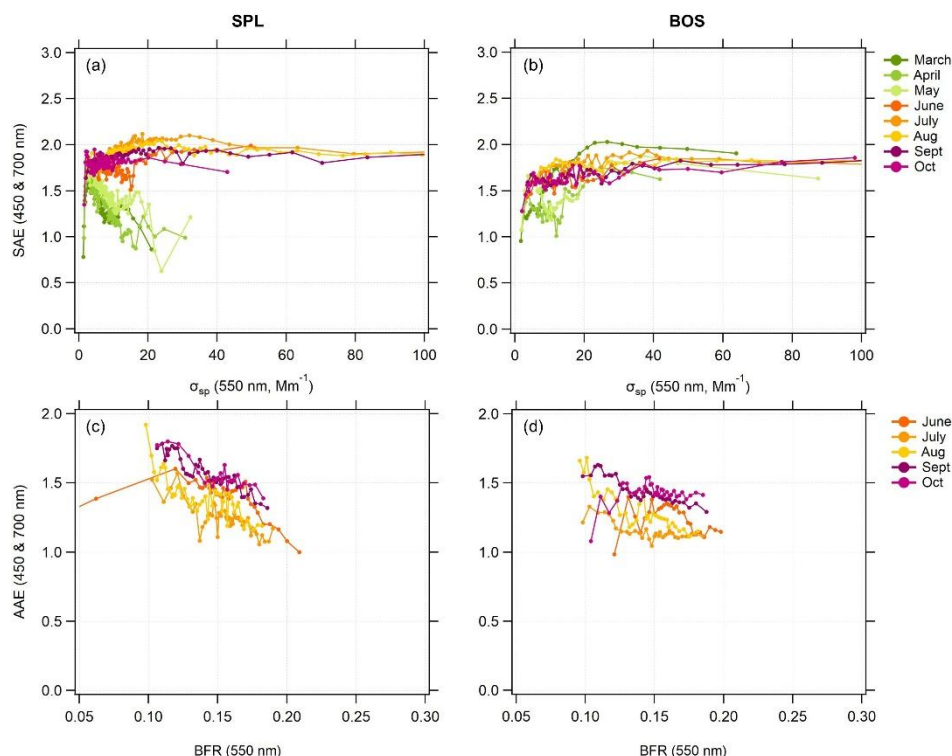
Figure 6. PM$_{10}$ SAE (450 & 700 nm) binned by σ$_{sp}$ (550 nm) for (a) SPL and (b) BOS. PM$_{10}$ AAE (450 & 700 nm) binned by the BFR (550 nm) for (c) SPL and (d) BOS. For all plots, each data point represents the median of 100 data points. Traces are colored by month with plots a & b showing data from March to September and plots c & d showing data from June to October. Fig. S14 presents the traces for all months.

The relationship between AAE and SAE has also been shown to be an indicator of aerosol type, and aerosol classification regimes have been established using these optical properties (Cappa et al., 2016; Cazorla et al., 2013). SAE is a good approximate indicator of the contribution of coarse mode aerosol, although other factors such as the shape of the size distribution might complicate the interpretation (Schuster et al., 2006). Looking at SAE in combination with AAE facilitates the differentiation of smoke and dust events, and since these are both clearly identifiable populations at SPL and BOS the use of this relationship is reasonable. However, these classifications can become less reliable as environmental conditions and source variability become more complex (Schmeisser et al., 2017). For this reason, these classifications are used to look at qualitative changes in aerosol classifications over time, between seasons, and during outlier events.

The classification scheme presented by Cappa et al. (2016) is used here. This scheme identifies eight aerosol regimes categorized primarily based on contributions from absorbing aerosol species (e.g., dust, BC, and brown carbon (BrC)) (**Fig. S14**). The classifications are labeled as: (1) dust, (2) mixed dust/BC/BrC, (3) large particle/BC mix, (4) large particle/low absorption mix or large black particles, (5) strong BrC, (6) mixed BC/BrC, (7) BC dominated, and (8) small particle/low absorption mix. The small particle/low absorption mix classification will not be discussed here as evidence suggests that data

in this category may be caused by high uncertainties at low signal levels (Cappa et al., 2016), and this category only represents
375 ~10% of the hourly data at both sites. BrC is often enhanced in wildfire smoke (Saleh et al., 2013), so categories 5 and 6 should
be more prominent during smoke events.

The largest cluster of data falls into the BC dominated classification, with 39% and 52% of the total hourly data
falling into this category at SPL and BOS, respectively. However, while the contribution of this category is relatively stable at
BOS (**Fig. S15**), its contribution to the aerosol population at SPL appears to be decreasing marginally (**Fig. S16**). This is
380 consistent with the overall decrease in aerosol at SPL shown in the trend analysis discussed above and indicates that the
background aerosol likely falls into this classification.

Clear seasonal differences exist in aerosol classification at both sites (**Fig. S17**, **Table S7**). In the springtime at SPL
the dominant aerosol classification changes to mixed dust/ BC/ BrC with 43 ± 18 % falling in this group. Instances of dust and
mixed dust/ BC/ BrC also appear to be increasing in the spring and winter at SPL. However, the number of data points in the
385 dust only class is small (on average ≤ 1 % of data in all seasons, **Table S7**). At BOS, the BC dominated class is still largest in
the spring, but the mixed dust/ BC/ BrC class is the second largest (**Table S7**) and influence from dust at BOS is clearly
increasing (**Fig. S15**). Looking specifically at extreme events in the spring, Fig. 7a and 7b show data where the daily average
σ_{sp} value was greater than or equal to the 90th percentile of the month; the points are colored by year. At SPL the AAE of
springtime events is increasing (**Fig. 7a**), which could indicate a trend towards less mixed or more extreme dust events. BOS
390 shows a clear shift in the class of springtime extreme events towards dust and mixed dust/ BC/ BrC categories (**Fig. 7b**).
Quantile regression on SAE at SPL also indicates a shift towards large particles in the spring, again consistent with and
increased dust contribution to aerosol loading.

In the summer and early fall (June – Sept), data at both sites is strongly clustered in the classifications influenced by
smaller BC and BrC particles (classes 5 – 7; **Fig. 7c**, **7d**, **S17**). These classes represent ~71% and ~87% of the data in the
395 summer and fall at SPL, and ~70% and ~73% of the data in the summer and fall at BOS. At SPL, the overall influence of the
mixed and strong BrC classifications is increasing in the summer and fall (**Fig. S16**). As previously mentioned, the contribution
of BC dominated aerosol is decreasing at SPL. However, the low magnitude of this trend is likely caused by the fact that both
background aerosol and aerosol from extreme events (**Fig. 7c**) are encompassed by this classification. Further chemical data
would be needed to parse the contributions and trends of the different aerosol sources. Changes in the contribution of these
400 classes at BOS are hard to discern given the shorter time span of the measurements. At both sites the extreme events during
the summer and early fall are also clustered into the smaller BC and BrC particle groups, which is further confirmation of
wildfire events during those months. Similar to the springtime, the AAE of events in the summer and early fall at SPL are
increasing and shifting classification towards more BrC influence. The summertime increase in AAE at SPL since the Japngie-
Green et al. (2019) study (i.e., **Fig. 5b**) in conjunction with the temporal changes in systematic variability shown in **Fig. 7** also
405 suggests an increase in the impact of smoke at SPL since 2016.
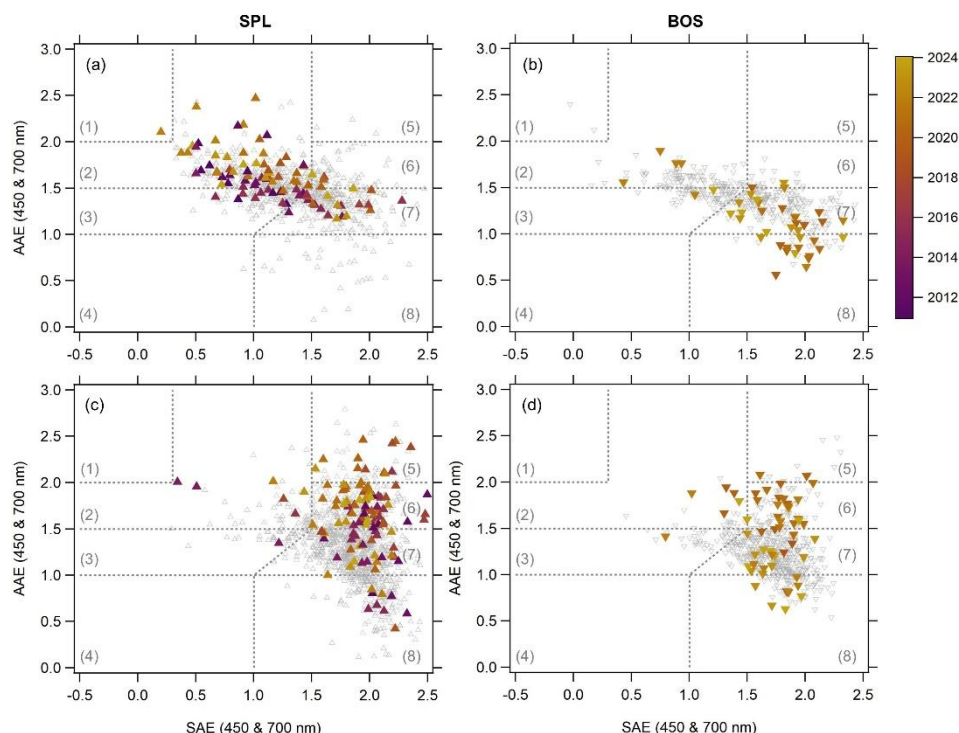
Figure 7. Daily medians of AAE vs SSA (450 & 700 nm) for March – May at (a) SPL and (b) BOS, and June – September for (c) SPL and (d) BOS. Open grey markers show all data, while closed colored markers show data where the daily average σ_{sp} value is greater than or equal to the 90th percentile for the month. The closed markers are colored by year, as indicated by the color scale. Different regimes defined by Cappa et al. (2016) are outlined using grey markers and are labeled one through eight, correlating to the numbered regimes found in the main text.

4 Conclusions

Changes to climate will impact aerosol loading in arid regions due to increases in both wildfire and dust emissions. In this study, long-term, ground-based aerosol optical data from two sites in Colorado (SPL and BOS) were analyzed. It was shown that wildfire activity has led to an increasing trend in extreme smoke events at SPL in the summer and fall months. Additionally, the analysis indicated an increase in the impact of dust aerosol at SPL in the spring. While the time series at BOS was insufficient for trend analysis, the temporal patterns and systematic variability among aerosol parameters were comparable to those at SPL. This suggests similar aerosol sources and timing at the two sites, although sources at BOS are clearly more mixed with anthropogenic emissions than at SPL.

Specifically, aerosol σ_{sp} and σ_{ap} peak in August at both SPL and BOS with July through September exhibiting higher loading than other times of year. This peak is attributed to wildfire smoke. Analysis of the long-term SPL time series indicates that there has been little change in the median summertime values of σ_{sp} (-0.3 ± 0.1 % y^{-1} at the 50th percentile). However, emissions from extreme events during the summer and fall have clearly increased with the σ_{sp} upper quartile range showing

425   significant positive trends (10 ± 1 % y^{-1} at the 98th percentile for summer). In contrast, upper quartile σ_{sp} data in the winter and spring exhibited small decreasing trends in loading (-2.4 ± 0.4 % y^{-1} at the 96th percentile for spring).

Systematic variability among aerosol optical properties was used to characterize sources of the aerosol. The relationship of SAE to σ_{sp} showed clear differences between spring (SAE decreases with scattering indicative of dust) and summer/fall (SAE increases with scattering consistent with smoke aerosol). AAE decreases with BFR – the high AAE/low

430   BFR points are characteristic of smoke particles, while the low AAE/high BFR are more representative of background aerosol. In the AAE vs SAE aerosol matrix developed by Cappa et al. (2016) there are seasonal shifts in the type of aerosol, with spring more likely to be impacted by dust and summer/fall more impacted by smoke, consistent with seasonal climatology, trend analyses and the systematic variability evaluation.

These findings highlight the importance of ongoing efforts to monitor and understand aerosol loading, variability,

435   and trends from natural and anthropogenic activities amidst a rapidly changing climate. Given the growing air quality concerns driven by enhanced wildfire and dust induced emissions, including health impacts and decreased visibility, continued monitoring and expanded analysis will be essential for improving our understanding of regional aerosol behavior under a changing climate.

440

Data avaliability. Aerosol optical data for both BOS and SPL is available through the EBAS database (https://ebas-data.nilu.no/Default.aspx). Fire data is from three different publicly accessible databases: Colorado data is from the Rocky Mountain Area Coordination Center annual reports (https://gacc.nifc.gov/rmcc/intelligence.php), national data for the USA is from the National Interagency Coordination Center (https://www.nifc.gov/nicc/predictive-services/intelligence), and national

445   data for Canada is from the Canadian Wildland Fire Information System (https://cwfis.cfs.nrcan.gc.ca/datamart). Topographic data used to construct Fig. 1 is from the Shuttle Radar Topography Mission described by Farr et al. (2007) (https://www.earthdata.nasa.gov/data/instruments/srtm/data-access-tools).

Author contributions. EKB performed the systematic variability analysis presented. EKB and AB prepared the manuscript

450   with contributions from all co-authors. AB did the initial climatology analysis for this work, with support from DK, JR, EA, & AGH. GC preformed all trend analysis presented. Data for this work was collected and quality controlled by AGH & GC for SPL and by EKB & EA for BOS. All authors reviewed and edited the manuscript.

Competing interests. At least one of the (co-)authors is a member of the editorial board of Atmospheric Chemistry and Physics.

455

Acknowledgements. We would like to acknowledge Storm Peak Laboratory, and NOAA Global Monitoring Laboratory for providing tech support, data protocols, and for maintaining the instruments that were used to collect the data for this project. EB and EA were supported by NOAA cooperative agreement NA22OAR4320151. Many have provided extensive

technical support over the years for Storm Peak Laboratory's instrumentation and data management. A special
460 acknowledgement goes to Mr. Dan Gilchrist, Dr. Maria Garcia, Mr. Ty Atkins, Ms. Megan Ostlie, and Mr. Joe Messina for all
their technical assistance with aerosol optical property measurements at SPL. Storm Peak Laboratory is a permittee of the
Medicine-Bow Routt National Forests and is an equal opportunity service provider and employer. Finally, the operations of
Storm Peak Laboratory would not be possible without the support of the Steamboat Ski and Resort Corporation for logistical
assistance and in-kind donations. Storm Peak Laboratory is supported by the National Science Foundation grant number
465 2113201, as a CIF. Patrick Sheridan and Jim Wendell were instrumental in getting the Table Mountain site set up in 2019 and
Derek Hageman's software for data acquisition, data QC and data archiving for both BOS and SPL makes doing science with
the data a joy. DK was supported by the Joint Fire Science Program and JR was supported by the Massachusetts Department
of Conservation and Recreation.

470

References

Achakulwisut, P., Anenberg, S. C., Neumann, J. E., Penn, S. L., Weiss, N., Crimmins, A., Fann, N., Martinich, J., Roman, H., and Mickley, L. J.: Effects of Increasing Aridity on Ambient Dust and Public Health in the U.S. Southwest Under Climate Change, GeoHealth, 3, 127–144, https://doi.org/10.1029/2019GH000187, 2019.

475 Anderson, T. L. and Ogren, J. A.: Determining Aerosol Radiative Properties Using the TSI 3563 Integrating Nephelometer, Aerosol Sci. Technol, 29, 57–69, https://doi.org/10.1080/02786829808965551, 1998.

Andrews, E., Sheridan, P. J., Ogren, J. A., and Ferrare, R.: In situ aerosol profiles over the Southern Great Plains cloud and radiation test bed site: 1. Aerosol optical properties, J. Geophys. Res., 109, https://doi.org/10.1029/2003JD004025, 2004.

Andrews, E., Ogren, J. A., Bonasoni, P., Marinoni, A., Cuevas, E., Rodríguez, S., Sun, J. Y., Jaffe, D. A., Fischer, E. V.,
480 Baltensperger, U., Weingartner, E., Coen, M. C., Sharma, S., Macdonald, A. M., Leaitch, W. R., Lin, N.-H., Laj, P., Arsov, T., Kalapov, I., Jefferson, A., and Sheridan, P.: Climatology of aerosol radiative properties in the free troposphere, Atmos. Res., 102, 365–393, https://doi.org/10.1016/j.atmosres.2011.08.017, 2011.

Andrews, E., Sheridan, P. J., Ogren, J. A., Hageman, D., Jefferson, A., Wendell, J., Alástuey, A., Alados-Arboledas, L., Bergin, M., Ealo, M., Hallar, A. G., Hoffer, A., Kalapov, I., Keywood, M., Kim, J., Kim, S.-W., Kolonjari, F., Labuschagne, C., Lin,
485 N.-H., Macdonald, A., Mayol-Bracero, O. L., McCubbin, I. B., Pandolfi, M., Reisen, F., Sharma, S., Sherman, J. P., Sorribas, M., and Sun, J.: Overview of the NOAA/ESRL Federated Aerosol Network, Bull. Amer. Meteor. Soc., 100, 123–135, https://doi.org/10.1175/BAMS-D-17-0175.1, 2019.

Augustine, J. A., Hodges, G. B., Dutton, E. G., Michalsky, J. J., and Cornwall, C. R.: An aerosol optical depth climatology for NOAA's national surface radiation budget network (SURFRAD), J. Geohys. Res., 113,
490 https://doi.org/10.1029/2007JD009504, 2008.

Barry, K. R., Hill, T. C. J., Levin, E. J. T., Twohy, C. H., Moore, K. A., Weller, Z. D., Toohey, D. W., Reeves, M., Campos, T., Geiss, R., Schill, G. P., Fischer, E. V., Kreidenweis, S. M., and DeMott, P. J.: Observations of Ice Nucleating Particles in the Free Troposphere From Western US Wildfires, J. Geophys. Res., 126, https://doi.org/10.1029/2020JD033752, 2021.

Bergstrom, R. W., Pilewskie, P., Russell, P. B., Redemann, J., Bond, T. C., Quinn, P. K., and Sierau, B.: Spectral absorption
495 properties of atmospheric aerosols, Atmos. Chem. Phys., 7, 5937–5943, https://doi.org/10.5194/acp-7-5937-2007, 2007.

Berner, A., Lürzer, Ch., Pohl, F., Preining, O., and Wagner, P.: The size distribution of the urban aerosol in Vienna, Sci. Total Environ., 13, 245–261, https://doi.org/10.1016/0048-9697(79)90105-0, 1979.

Bian, Q., Ford, B., Pierce, J. R., and Kreidenweis, S. M.: A Decadal Climatology of Chemical, Physical, and Optical Properties of Ambient Smoke in the Western and Southeastern United States, J. Geohys. Res., 125,
500 https://doi.org/10.1029/2019JD031372, 2020.

Bond, T. C., Anderson, T. L., and Campbell, D.: Calibration and Intercomparison of Filter-Based Measurements of Visible Light Absorption by Aerosols, Aerosol Sci. Technol, 30, 582–600, https://doi.org/10.1080/027868299304435, 1999.

Bond, T. C., Doherty, S. J., Fahey, D. W., Forster, P. M., Berntsen, T., DeAngelo, B. J., Flanner, M. G., Ghan, S., Kärcher, B., Koch, D., Kinne, S., Kondo, Y., Quinn, P. K., Sarofim, M. C., Schultz, M. G., Schulz, M., Venkataraman, C., Zhang, H.,
505 Zhang, S., Bellouin, N., Guttikunda, S. K., Hopke, P. K., Jacobson, M. Z., Kaiser, J. W., Klimont, Z., Lohmann, U., Schwarz, J. P., Shindell, D., Storelvmo, T., Warren, S. G., and Zender, C. S.: Bounding the role of black carbon in the climate system: A scientific assessment, J. Geohys. Res., 118, 5380–5552, https://doi.org/10.1002/jgrd.50171, 2013.

Borys, R. D. and Wetzel, M. A.: Storm Peak Laboratory: A Research, Teaching, and Service Facility for the Atmospheric Sciences, Bull. Am. Meteorol. Soc., 78, 2115–2123, https://doi.org/10.1175/1520-
510   0477(1997)078%253C2115:SPLART%253E2.0.CO;2, 1997.

Burke, M., Driscoll, A., Heft-Neal, S., Xue, J., Burney, J., and Wara, M.: The changing risk and burden of wildfire in the United States, Proc. Natl. Acad. Sci., 118, e2011048118, https://doi.org/10.1073/pnas.2011048118, 2021.

Cappa, C. D., Kolesar, K. R., Zhang, X., Atkinson, D. B., Pekour, M. S., Zaveri, R. A., Zelenyuk, A., and Zhang, Q.: Understanding the optical properties of ambient sub- and supermicron particulate matter: results from the CARES 2010 field
515   study in northern California, Atmos. Chem. Phys., 16, 6511–6535, https://doi.org/10.5194/acp-16-6511-2016, 2016.

Cazorla, A., Bahadur, R., Suski, K. J., Cahill, J. F., Chand, D., Schmid, B., Ramanathan, V., and Prather, K. A.: Relating aerosol absorption due to soot, organic carbon, and dust to emission sources determined from in-situ chemical measurements, Atmos. Chem. Phys., 13, 9337–9350, https://doi.org/10.5194/acp-13-9337-2013, 2013.

Clarke, A., McNaughton, C., Kapustin, V., Shinozuka, Y., Howell, S., Dibb, J., Zhou, J., Anderson, B., Brekhovskikh, V.,
520   Turner, H., and Pinkerton, M.: Biomass burning and pollution aerosol over North America: Organic components and their influence on spectral optical properties and humidification response, J. Geohys. Res., 112, https://doi.org/10.1029/2006JD007777, 2007.

Collaud Coen, M., Weingartner, E., Nyeki, S., Cozic, J., Henning, S., Verheggen, B., Gehrig, R., and Baltensperger, U.: Long-term trend analysis of aerosol variables at the high-alpine site Jungfraujoch, J. Geohys. Res., 112,
525   https://doi.org/10.1029/2006JD007995, 2007.

Collaud Coen, M., Andrews, E., Aliaga, D., Andrade, M., Angelov, H., Bukowiecki, N., Ealo, M., Fialho, P., Flentje, H., Hallar, A. G., Hooda, R., Kalapov, I., Krejci, R., Lin, N.-H., Marinoni, A., Ming, J., Nguyen, N. A., Pandolfi, M., Pont, V., Ries, L., Rodríguez, S., Schauer, G., Sellegri, K., Sharma, S., Sun, J., Tunved, P., Velasquez, P., and Ruffieux, D.: Identification of topographic features influencing aerosol observations at high altitude stations, Atmos. Chem. Phys., 18,
530   12289–12313, https://doi.org/10.5194/acp-18-12289-2018, 2018.

Collaud Coen, M., Andrews, E., Alastuey, A., Arsov, T. P., Backman, J., Brem, B. T., Bukowiecki, N., Couret, C., Eleftheriadis, K., Flentje, H., Fiebig, M., Gysel-Beer, M., Hand, J. L., Hoffer, A., Hooda, R., Hueglin, C., Joubert, W., Keywood, M., Kim, J. E., Kim, S.-W., Labuschagne, C., Lin, N.-H., Lin, Y., Lund Myhre, C., Luoma, K., Lyamani, H., Marinoni, A., Mayol-Bracero, O. L., Mihalopoulos, N., Pandolfi, M., Prats, N., Prenni, A. J., Putaud, J.-P., Ries, L., Reisen,
535   F., Sellegri, K., Sharma, S., Sheridan, P., Sherman, J. P., Sun, J., Titos, G., Torres, E., Tuch, T., Weller, R., Wiedensohler, A., Zieger, P., and Laj, P.: Multidecadal trend analysis of in situ aerosol radiative properties around the world, Atmos. Chem. Phys., 20, 8867–8908, https://doi.org/10.5194/acp-20-8867-2020, 2020.

Creamean, J. M., Neiman, P. J., Coleman, T., Senff, C. J., Kirgis, G., Alvarez, R. J., and Yamamoto, A.: Colorado air quality impacted by long-range-transported aerosol: a set ofcase studies during the 2015 Pacific Northwest fires, Atmos. Chem. Phys.,
540   16, 12329–12345, https://doi.org/10.5194/acp-16-12329-2016, 2016.

Davulienė, L., Janicka, L., Minderytė, A., Kalinauskaitė, A., Poczta, P., Karasewicz, M., Hafiz, A., Pashneva, D., Dudoitis, V., Kandrotaitė, K., Valiulis, D., Böckmann, C., Schüttemeyer, D., Stachlewska, I. S., and Byčenkienė, S.: Synergic use of in-situ and remote sensing techniques for comprehensive characterization of aerosol optical and microphysical properties, Sci. Total Environ., 906, 167585, https://doi.org/10.1016/j.scitotenv.2023.167585, 2024.

545   Delfino, R. J., Brummel, S., Wu, J., Stern, H., Ostro, B., Lipsett, M., Winer, A., Street, D. H., Zhang, L., Tjoa, T., and Gillen, D. L.: The relationship of respiratory and cardiovascular hospital admissions to the southern California wildfires of 2003, Occup. Environ. Med., 66, 189–197, https://doi.org/10.1136/oem.2008.041376, 2009.

Dennison, P. E., Brewer, S. C., Arnold, J. D., and Moritz, M. A.: Large wildfire trends in the western United States, 1984–2011, Geophys. Res. Lett., 41, 2928–2933, https://doi.org/10.1002/2014GL059576, 2014.

550 Eibedingil, I. G., Gill, T. E., Van Pelt, R. S., and Tong, D. Q.: Comparison of Aerosol Optical Depth from MODIS Product Collection 6.1 and AERONET in the Western United States, Remote Sens., 13, 2316, https://doi.org/10.3390/rs13122316, 2021.

Farr, T. G., Rosen, P. A., Caro, E., Crippen, R., Duren, R., Hensley, S., Kobrick, M., Paller, M., Rodriguez, E., Roth, L., Seal, D., Shaffer, S., Shimada, J., Umland, J., Werner, M., Oskin, M., Burbank, D., and Alsdorf, D.: The Shuttle Radar Topography 555 Mission, Rev. Geophys., 45, https://doi.org/10.1029/2005RG000183, 2007.

Ford, B., Val Martin, M., Zelasky, S. E., Fischer, E. V., Anenberg, S. C., Heald, C. L., and Pierce, J. R.: Future Fire Impacts on Smoke Concentrations, Visibility, and Health in the Contiguous United States, GeoHealth, 2, 229–247, https://doi.org/10.1029/2018GH000144, 2018.

Forrister, H., Liu, J., Scheuer, E., Dibb, J., Ziemba, L., Thornhill, K. L., Anderson, B., Diskin, G., Perring, A. E., Schwarz, J. 560 P., Campuzano-Jost, P., Day, D. A., Palm, B. B., Jimenez, J. L., Nenes, A., and Weber, R. J.: Evolution of brown carbon in wildfire plumes, Geophys. Res. Lett., 42, 4623–4630, https://doi.org/10.1002/2015GL063897, 2015.

Ghan, S. J. and Schwartz, S. E.: Aerosol Properties and Processes: A Path from Field and Laboratory Measurements to Global Climate Models, Bull. Amer. Meteor. Soc, 88, 1059–1084, https://doi.org/10.1175/BAMS-88-7-1059, 2007.

Goss, M., Swain, D. L., Abatzoglou, J. T., Sarhadi, A., Kolden, C. A., Williams, A. P., and Diffenbaugh, N. S.: Climate change 565 is increasing the likelihood of extreme autumn wildfire conditions across California, Environ. Res. Lett., 15, 094016, https://doi.org/10.1088/1748-9326/ab83a7, 2020.

Haikerwal, A., Akram, M., Sim, M. R., Meyer, M., Abramson, M. J., and Dennekamp, M.: Fine particulate matter (PM2.5) exposure during a prolonged wildfire period and emergency department visits for asthma, Respirology (Carlton, Vic.), 21, 88–94, https://doi.org/10.1111/resp.12613, 2016.

570 Hallar, A. G., Petersen, R., Andrews, E., Michalsky, J., McCubbin, I. B., and Ogren, J. A.: Contributions of dust and biomass burning to aerosols at a Colorado mountain-top site, Atmos. Chem. Phys., 15, 13665–13679, https://doi.org/10.5194/acp-15-13665-2015, 2015.

Hallar, A. G., Molotch, N. P., Hand, J. L., Livneh, B., McCubbin, I. B., Petersen, R., Michalsky, J., Lowenthal, D., and Kunkel, K. E.: Impacts of increasing aridity and wildfires on aerosol loading in the intermountain Western US, Environ. Res. Lett., 12, 575 014006, https://doi.org/10.1088/1748-9326/aa510a, 2017.

Hallar, A. G., McCubbin, I. B., Borys, R., Lowenthal, D. H., Wetzel, M., Hindman, E., Brooks, S. D., Steenburgh, W. J., Gratz, L., Hoch, S., Stephens, B., Horel, J. D., Molotch, N. P., Mace, G. G., Bailey, A., Pettersen, C., Andrews, E., Cziczo, D. J., and Garcia, M.: Storm Peak Laboratory: A Research and Training Facility for the Atmospheric Sciences, Bull. Amer. Meteor. Soc., 106, E1130–E1148, https://doi.org/10.1175/BAMS-D-24-0043.1, 2025.

580 Hand, J. L., Gill, T. E., and Schichtel, B. A.: Urban and rural coarse aerosol mass across the United States: Spatial and seasonal variability and long-term trends, Atmos. Environ., 218, 117025, https://doi.org/10.1016/j.atmosenv.2019.117025, 2019.

Hand, J. L., Prenni, A. J., Copeland, S., Schichtel, B. A., and Malm, W. C.: Thirty years of the Clean Air Act Amendments: Impacts on haze in remote regions of the United States (1990–2018), Atmos. Environ., 243, 117865, https://doi.org/10.1016/j.atmosenv.2020.117865, 2020.

585   Hand, J. L., Prenni, A. J., Raffuse, S. M., Hyslop, N. P., Malm, W. C., and Schichtel, B. A.: Spatial and Seasonal Variability
       of Remote and Urban Speciated Fine Particulate Matter in the United States, J. Geophys. Res., 129, e2024JD042579,
       https://doi.org/10.1029/2024JD042579, 2024.

       Higuera, P. E. and Abatzoglou, J. T.: Record-setting climate enabled the extraordinary 2020 fire season in the western United
       States, Glob. Change Biol., 27, 1–2, https://doi.org/10.1111/gcb.15388, 2021.

590   Iglesias, V., Balch, J. K., and Travis, W. R.: U.S. fires became larger, more frequent, and more widespread in the 2000s, Sci.
       Adv., 8, eabc0020, https://doi.org/10.1126/sciadv.abc0020, 2022.

       Intergovernmental Panel on Climate Change (IPCC): Climate Change 2021 – The Physical Science Basis: Working Group I
       Contribution to the Sixth Assessment Report of the Intergovernmental Panel on Climate Change, Cambridge University Press,
       https://doi.org/10.1017/9781009157896, 2023.

595   Jahn, L. G., Polen, M. J., Jahl, L. G., Brubaker, T. A., Somers, J., and Sullivan, R. C.: Biomass combustion produces ice-active
       minerals in biomass-burning aerosol and bottom ash, Proc. Natl. Acad. Sci. U. S. A., 117, 21928–21937,
       https://doi.org/10.1073/pnas.1922128117, 2020.

       Japngie-Green, C. M., Andrews, E., McCubbin, I. B., Ogren, J. A., and Hallar, A. G.: Climatology of Aerosol Optical
       Properties at Storm Peak Laboratory, Aerosol Air Qual. Res., 19, 1205–1213, https://doi.org/10.4209/aaqr.2018.05.0204,
600   2019.

       Jiang, Y., Yang, X.-Q., Liu, X., Qian, Y., Zhang, K., Wang, M., Li, F., Wang, Y., and Lu, Z.: Impacts of Wildfire Aerosols on
       Global Energy Budget and Climate: The Role of Climate Feedbacks, J. Climate, 33, 3351–3366, https://doi.org/10.1175/JCLI-
       D-19-0572.1, 2020.

       Johnston, F. H., Henderson, S. B., Chen, Y., Randerson, J. T., Marlier, M., Defries, R. S., Kinney, P., Bowman, D. M. J. S.,
605   and Brauer, M.: Estimated global mortality attributable to smoke from landscape fires, Environ. Health Perspect., 120, 695–
       701, https://doi.org/10.1289/ehp.1104422, 2012.

       Junghenn Noyes, K. T., Kahn, R. A., Limbacher, J. A., and Li, Z.: Canadian and Alaskan wildfire smoke particle properties,
       their evolution, and controlling factors, from satellite observations, Atmos. Chem. Phys., 22, 10267–10290,
       https://doi.org/10.5194/acp-22-10267-2022, 2022.

610   Koenker, R.: Quantile Regression, Cambridge University Press, Cambridge, https://doi.org/10.1017/CBO9780511754098,
       2005.

       Koenker, R. and Bassett, G.: Regression Quantiles, Econometrica, 46, 33–50, https://doi.org/10.2307/1913643, 1978.

       Koenker, R. and Hallock, K. F.: Quantile Regression, J. Econ. Perspect., 15, 143–156, https://doi.org/10.1257/jep.15.4.143,
       2001.

615   Koenker, R. W. and D'Orey, V.: Computing Regression Quantiles, J. R. Stat. Soc. Ser. C. Appl. Stat., 36, 383–393,
       https://doi.org/10.2307/2347802, 1987.

       Kok, J. F., Storelvmo, T., Karydis, V. A., Adebiyi, A. A., Mahowald, N. M., Evan, A. T., He, C., and Leung, D. M.: Mineral
       dust aerosol impacts on global climate and climate change, Nat Rev Earth Environ, 4, 71–86, https://doi.org/10.1038/s43017-
       022-00379-5, 2023.

620   Laj, P., Bigi, A., Rose, C., Andrews, E., Lund Myhre, C., Collaud Coen, M., Lin, Y., Wiedensohler, A., Schulz, M., Ogren, J. A., Fiebig, M., Gliß, J., Mortier, A., Pandolfi, M., Petäja, T., Kim, S.-W., Aas, W., Putaud, J.-P., Mayol-Bracero, O., Keywood, M., Labrador, L., Aalto, P., Ahlberg, E., Alados Arboledas, L., Alastuey, A., Andrade, M., Artíñano, B., Ausmeel, S., Arsov, T., Asmi, E., Backman, J., Baltensperger, U., Bastian, S., Bath, O., Beukes, J. P., Brem, B. T., Bukowiecki, N., Conil, S., Couret, C., Day, D., Dayantolis, W., Degorska, A., Eleftheriadis, K., Fetfatzis, P., Favez, O., Flentje, H., Gini, M. I., Gregorič,
625   A., Gysel-Beer, M., Hallar, A. G., Hand, J., Hoffer, A., Hueglin, C., Hooda, R. K., Hyvärinen, A., Kalapov, I., Kalivitis, N., Kasper-Giebl, A., Kim, J. E., Kouvarakis, G., Kranjc, I., Krejci, R., Kulmala, M., Labuschagne, C., Lee, H.-J., Lihavainen, H., Lin, N.-H., Löschau, G., Luoma, K., Marinoni, A., Martins Dos Santos, S., Meinhardt, F., Merkel, M., Metzger, J.-M., Mihalopoulos, N., Nguyen, N. A., Ondracek, J., Pérez, N., Perrone, M. R., Petit, J.-E., Picard, D., Pichon, J.-M., Pont, V., Prats, N., Prenni, A., Reisen, F., Romano, S., Sellegri, K., Sharma, S., Schauer, G., Sheridan, P., Sherman, J. P., Schütze, M.,
630   Schwerin, A., Sohmer, R., Sorribas, M., Steinbacher, M., Sun, J., Titos, G., et al.: A global analysis of climate-relevant aerosol properties retrieved from the network of Global Atmosphere Watch (GAW) near-surface observatories, Atmos. Meas. Tech., 13, 4353–4392, https://doi.org/10.5194/amt-13-4353-2020, 2020.

Lambert, A., Hallar, A. G., Garcia, M., Strong, C., Andrews, E., and Hand, J. L.: Dust Impacts of Rapid Agricultural Expansion on the Great Plains, Geophys. Res. Lett., 47, e2020GL090347, https://doi.org/10.1029/2020GL090347, 2020.

635   Lee, S., Yoon, S.-C., Kim, S.-W., Kim, Y. P., Ghim, Y. S., Kim, J.-H., Kang, C.-H., Kim, Y. J., Chang, L.-S., and Lee, S.-J.: Spectral dependency of light scattering/absorption and hygroscopicity of pollution and dust aerosols in Northeast Asia, Atmos. Environ., 50, 246–254, https://doi.org/10.1016/j.atmosenv.2011.12.026, 2012.

Leeper, R. D., Bilotta, R., Petersen, B., Stiles, C. J., Heim, R., Fuchs, B., Prat, O. P., Palecki, M., and Ansari, S.: Characterizing U.S. drought over the past 20 years using the U.S. drought monitor, Int. J. Climatol., 42, 6616–6630,
640   https://doi.org/10.1002/joc.7653, 2022.

Lian, X., Piao, S., Li, L. Z. X., Li, Y., Huntingford, C., Ciais, P., Cescatti, A., Janssens, I. A., Peñuelas, J., Buermann, W., Chen, A., Li, X., Myneni, R. B., Wang, X., Wang, Y., Yang, Y., Zeng, Z., Zhang, Y., and McVicar, T. R.: Summer soil drying exacerbated by earlier spring greening of northern vegetation, Sci. Adv., 6, eaax0255, https://doi.org/10.1126/sciadv.aax0255, 2020.

645   Liu, J. C., Pereira, G., Uhl, S. A., Bravo, M. A., and Bell, M. L.: A systematic review of the physical health impacts from non-occupational exposure to wildfire smoke, Environ. Res., 136, 120–132, https://doi.org/10.1016/j.envres.2014.10.015, 2015.

Liu, J. C., Wilson, A., Mickley, L. J., Dominici, F., Ebisu, K., Wang, Y., Sulprizio, M. P., Peng, R. D., Yue, X., Son, J.-Y., Anderson, G. B., and Bell, M. L.: Wildfire-specific Fine Particulate Matter and Risk of Hospital Admissions in Urban and Rural Counties, Epidemiology (Cambridge, Mass.), 28, 77–85, https://doi.org/10.1097/EDE.0000000000000556, 2017.

650   Malm, W. C., Schichtel, B. A., Prenni, A. J., Day, D., Andrews, E., Perkins, R., Sullivan, A., and Tigges, M.: Revisiting integrating nephelometer measurements, Atmos. Environ., 319, 120237, https://doi.org/10.1016/j.atmosenv.2023.120237, 2024.

McClure, C. D. and Jaffe, D. A.: US particulate matter air quality improves except in wildfire-prone areas, Proc. Natl. Acad. Sci. U. S. A., 115, 7901–7906, https://doi.org/10.1073/pnas.1804353115, 2018.

655   Mote, P. W., Li, S., Lettenmaier, D. P., Xiao, M., and Engel, R.: Dramatic declines in snowpack in the western US, npj Clim Atmos Sci, 1, 2, https://doi.org/10.1038/s41612-018-0012-1, 2018.

Ogren, J. A.: Comment on "Calibration and Intercomparison of Filter-Based Measurements of Visible Light Absorption by Aerosols," Aerosol Sci. Technol, 44, 589–591, https://doi.org/10.1080/02786826.2010.482111, 2010.

660 Ogren, J. A., Wendell, J., Andrews, E., and Sheridan, P. J.: Continuous light absorption photometer for long-term studies, Atmos. Meas. Tech., 10, 4805–4818, https://doi.org/10.5194/amt-10-4805-2017, 2017.

Pederson, G. T., Betancourt, J. L., and McCabe, G. J.: Regional patterns and proximal causes of the recent snowpack decline in the Rocky Mountains, U.S., Geophys. Res. Lett., 40, 1811–1816, https://doi.org/10.1002/grl.50424, 2013.

Penner, J. E., Dickinson, R. E., and O'Neill, C. A.: Effects of Aerosol from Biomass Burning on the Global Radiation Budget, Science, 256, 1432–1434, https://doi.org/10.1126/science.256.5062.1432, 1992.

665 Pu, B. and Ginoux, P.: Projection of American dustiness in the late 21st century due to climate change, Sci Rep, 7, 5553, https://doi.org/10.1038/s41598-017-05431-9, 2017.

quantreg, Koenker, R., Portnoy, S., Ng, P. T., Melly, B., Zeileis, A., Grosjean, P., Moler, C., Saad, Y., Chernozhukov, V., Fernandez-Val, I., Maechler, M., and Ripley, B. D.: Quantile Regression, R [code], https://doi.org/10.32614/CRAN.package.quantreg, 2025.

670 Russell, P. B., Bergstrom, R. W., Shinozuka, Y., Clarke, A. D., DeCarlo, P. F., Jimenez, J. L., Livingston, J. M., Redemann, J., Dubovik, O., and Strawa, A.: Absorption Angstrom Exponent in AERONET and related data as an indicator of aerosol composition, Atmos. Chem. Phys., 10, 1155–1169, https://doi.org/10.5194/acp-10-1155-2010, 2010.

Saleh, R., Hennigan, C. J., McMeeking, G. R., Chuang, W. K., Robinson, E. S., Coe, H., Donahue, N. M., and Robinson, A. L.: Absorptivity of brown carbon in fresh and photo-chemically aged biomass-burning emissions, Atmos. Chem. Phys., 13, 675 7683–7693, https://doi.org/10.5194/acp-13-7683-2013, 2013.

Schmeisser, L., Andrews, E., Ogren, J. A., Sheridan, P., Jefferson, A., Sharma, S., Kim, J. E., Sherman, J. P., Sorribas, M., Kalapov, I., Arsov, T., Angelov, C., Mayol-Bracero, O. L., Labuschagne, C., Kim, S.-W., Hoffer, A., Lin, N.-H., Chia, H.-P., Bergin, M., Sun, J., Liu, P., and Wu, H.: Classifying aerosol type using in situ surface spectral aerosol optical properties, Atmos. Chem. Phys., 17, 12097–12120, https://doi.org/10.5194/acp-17-12097-2017, 2017.

680 Schuster, G. L., Dubovik, O., and Holben, B. N.: Angstrom exponent and bimodal aerosol size distributions, J. Geophys. Res., 111, https://doi.org/10.1029/2005JD006328, 2006.

Seinfeld, J. H. and Pandis, S. N.: Atmospheric chemistry and physics: from air pollution to climate change, 2nd ed., Johm Wiley & Sons, New York, 2006.

Selimovic, V., Yokelson, R. J., Warneke, C., Roberts, J. M., de Gouw, J., Reardon, J., and Griffith, D. W. T.: Aerosol optical 685 properties and trace gas emissions by PAX and OP-FTIR for laboratory-simulated western US wildfires during FIREX, Atmos. Chem. Phys., 18, 2929–2948, https://doi.org/10.5194/acp-18-2929-2018, 2018.

Sherman, J. P., Sheridan, P. J., Ogren, J. A., Andrews, E., Hageman, D., Schmeisser, L., Jefferson, A., and Sharma, S.: A multi-year study of lower tropospheric aerosol variability and systematic relationships from four North American regions, Atmos. Chem. Phys., 15, 12487–12517, https://doi.org/10.5194/acp-15-12487-2015, 2015.

690 Twohy, C. H., Toohey, D. W., Levin, E. J. T., DeMott, P. J., Rainwater, B., Garofalo, L. A., Pothier, M. A., Farmer, D. K., Kreidenweis, S. M., Pokhrel, R. P., Murphy, S. M., Reeves, J. M., Moore, K. A., and Fischer, E. V.: Biomass Burning Smoke and Its Influence on Clouds Over the Western U. S., Geophys. Res. Lett., 48, e2021GL094224, https://doi.org/10.1029/2021GL094224, 2021.

Val Martin, M., Heald, C. L., Ford, B., Prenni, A. J., and Wiedinmyer, C.: A decadal satellite analysis of the origins and 695 impacts of smoke in Colorado, Atmos. Chem. Phys., 13, 7429–7439, https://doi.org/10.5194/acp-13-7429-2013, 2013.

Weber, K. T. and Yadav, R.: Spatiotemporal Trends in Wildfires across the Western United States (1950–2019), Remote Sens., 12, 2959, https://doi.org/10.3390/rs12182959, 2020.

Wei, J., Li, Z., Peng, Y., and Sun, L.: MODIS Collection 6.1 aerosol optical depth products over land and ocean: validation and comparison, Atmos. Environ., 201, 428–440, https://doi.org/10.1016/j.atmosenv.2018.12.004, 2019.

Westerling, A. L., Hidalgo, H. G., Cayan, D. R., and Swetnam, T. W.: Warming and Earlier Spring Increase Western U.S. Forest Wildfire Activity, Science, 313, 940–943, https://doi.org/10.1126/science.1128834, 2006.

Wilmot, T. Y., Hallar, A. G., Lin, J. C., and Mallia, D. V.: Expanding number of Western US urban centers face declining summertime air quality due to enhanced wildland fire activity, Environ. Res. Lett., 16, 054036, https://doi.org/10.1088/1748-9326/abf966, 2021.

WMO: WMO/GAW Aerosol Measurement Procedures, Guidelines and Recommendations, Report No. 227, World Meteorological Organization, Geneva, Switzerland, 2016.

Yokelson, R. J., Crounse, J. D., DeCarlo, P. F., Karl, T., Urbanski, S., Atlas, E., Campos, T., Shinozuka, Y., Kapustin, V., Clarke, A. D., Weinheimer, A., Knapp, D. J., Montzka, D. D., Holloway, J., Weibring, P., Flocke, F., Zheng, W., Toohey, D., Wennberg, P. O., Wiedinmyer, C., Mauldin, L., Fried, A., Richter, D., Walega, J., Jimenez, J. L., Adachi, K., Buseck, P. R., Hall, S. R., and Shetter, R.: Emissions from biomass burning in the Yucatan, Atmos. Chem. Phys., 9, 5785–5812, https://doi.org/10.5194/acp-9-5785-2009, 2009.